THE JOURNAL OF PHYSICAL CHEMISTRY Letters

Letter

pubs.acs.org/JPCL

Harnessing Excited-State Intramolecular Proton-Transfer Reaction via a Series of Amino-Type Hydrogen-Bonding Molecules

Huan-Wei Tseng,[†] Jun-Qi Liu,[‡] Yi-An Chen,[†] Chi-Min Chao,*[,‡,§] Kuan-Miao Liu,*[,‡,§] Chi-Lin Chen,[†] Tzu-Chieh Lin,[†] Cheng-Hsien Hung,[‡] Yen-Lin Chou,[‡] Ta-Chun Lin,[‡] Tian-Lin Wang,[†] and Pi-Tai Chou*[,†]

[†]Department of Chemistry, National Taiwan University, Taipei 10617, Taiwan

[‡]School of Medical Applied Chemistry, Chung Shan Medical University, Taichung 40201, Taiwan

[§]Department of Medical Education, Chung Shan Medical University Hospital, Taichung 40201, Taiwan

Supporting Information

ABSTRACT: A series of new amino (NH)-type hydrogen-bonding (H-bonding) compounds comprising 2-(2′-aminophenyl)-benzothiazole and its extensive derivatives were designed and synthesized. Unlike in the hydroxyl (OH)-type H-bonding systems, one of the amino hydrogens can be replaced with electron-donating/withdrawing groups. This, together with a versatile capability for modifying the parent moiety, makes feasible the comprehensive spectroscopy and dynamics studies of amino-type excited-state intramolecular proton transfer (ESIPT), which was previously inaccessible in the hydroxyl-type ESIPT systems. Empirical correlations were observed among the hydrogen-bonding strength (the N−H bond distances and proton acidity), ESIPT kinetics, and thermodynamics, demonstrating a trend that the stronger N−H···N hydrogen bond leads to a faster ESIPT, as experimentally observed, and a more exergonic reaction thermodynamics. Accordingly, ESIPT reaction can be harnessed for the first time from a highly endergonic type (i.e., prohibition) toward equilibrium with a measurable ESIPT rate and then to the highly exergonic, ultrafast ESIPT reaction within the same series of amino-type intramolecular H-bond system.

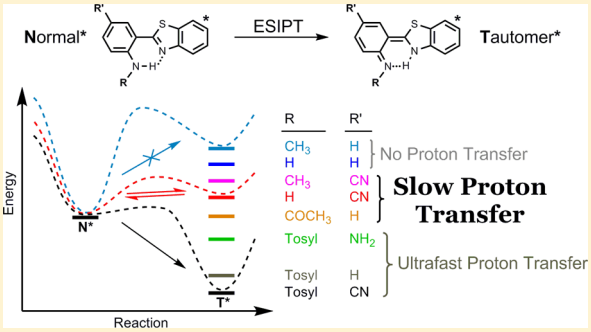

Excited-state intramolecular proton transfer (ESIPT) reaction has been receiving considerable attention. In sharp contrast to the multitude of papers reporting hydroxyl-type ESIPT,[1−3] a search of the literature indicates that only a few reports have dealt with amino-type ESIPT using primary amines as proton donors.[4−12] The scarcity of relevant reports is due to the much weaker intramolecular hydrogen bond (H-bond) associated with the amino N−H proton (cf. the O−H type H-bond). In the electronic ground state, the amino proton (as in aniline) has much weaker acidity ($pK_a > 30$)[13] than the hydroxyl proton in, for example, phenol ($pK_a \approx 10$).[14] A similar acidity trend is expected in the electronically excited state; therefore, ESIPT rarely takes place in N−H H-bonding systems unless the acidity of the N−H proton can be enhanced via suitable chemical modification. This has been done mostly by replacing one of the N−H protons with an electron-withdrawing tosyl (Ts) group or an acetyl (Ac) group, forming Ts−N−H or Ac−N−H, to increase the N−H acidity.[9−12] The prerequisites of such chemical modification are not trivial and thus have not received much attention from physical chemists and/or spectroscopists. As a result, most of the relevant works to date have been reported by synthetic and material chemists focusing on the synthetic routes, the corresponding steady-state absorption/emission spectra, and the population lifetime, whereas in-depth insights into the dynamics of N−H ESIPT unfortunately are still lacking.

The similarities and differences in the ESIPT mechanism between N−H and O−H H-bonding systems are apparently a key fundamental issue. While O−H cannot undergo any further chemical modification, the versatility of the −N(R)−H group, where R can be endowed with various functionalities, may provide unprecedented opportunities for harnessing the ESIPT in terms of dynamics and/or thermodynamics and eventually the modulation of ratiometric (normal versus proton-transfer) emission, which could shed light on fundamental and corresponding applications.

Molecules such as 2-(2′-hydroxyphenyl)benzimidazole (**HBI**),[15−18] 2-(2′-hydroxyphenyl)benzoxazole (**HBO**),[19−22] and 2-(2′-hydroxyphenyl)benzothiazole (**HBT**)[23−25] with benzazole scaffolds have been extensively investigated for the O−H-type ESIPT. For a direct and fair comparison, we thus adopted the benzazole moiety as the H-bond acceptor in the design of our system for the study of N−H-type ESIPT. Because benzimidazole (two nitrogen atoms) and benzoxazole

Received: February 27, 2015
Accepted: April 1, 2015
Published: April 1, 2015

DOI: 10.1021/acs.jpclett.5b00423
J. Phys. Chem. Lett. 2015, 6, 1477−1486

Scheme 1. Synthetic Routes for the Titled Compounds in This Study

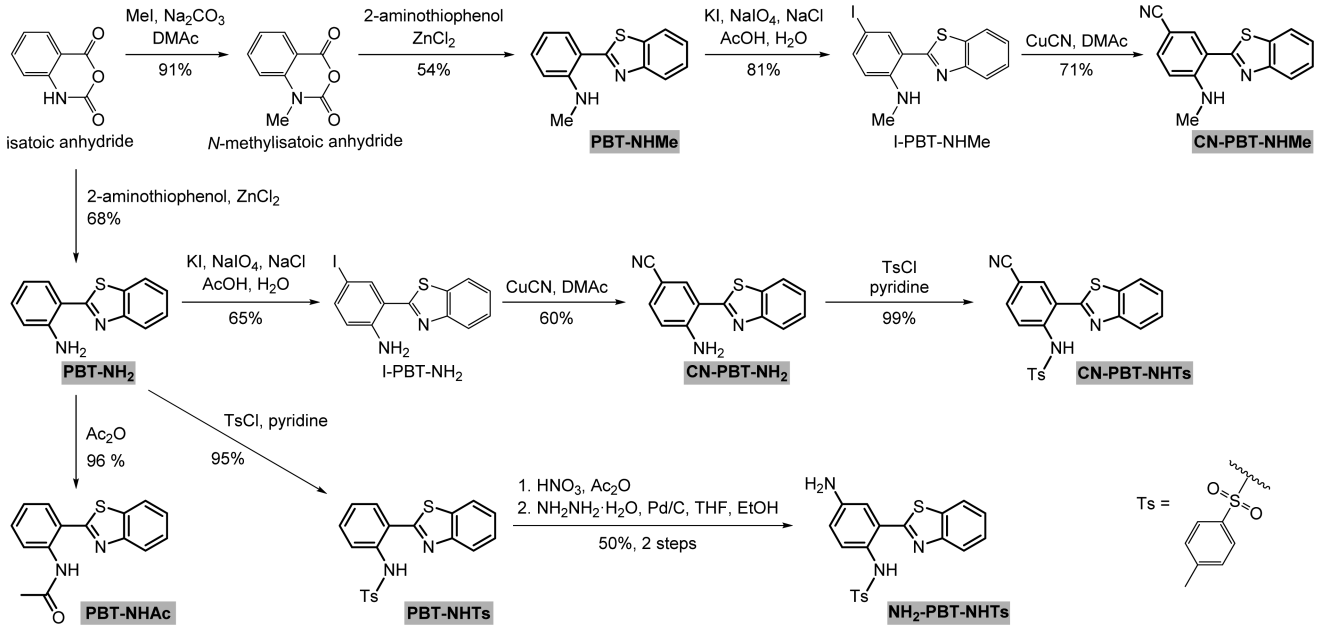

(one nitrogen atom and one oxygen atom) moieties provide two H-bond acceptors that complicate the proton-transfer behavior, we thus simplified the situation by choosing benzothiazole as the moiety (see Scheme 1).

Herein, we report the synthesis and comprehensive photophysical studies of a new series of amino-type intramolecular H-bonding systems bearing the benzothiazole chromophore. In this study, the −R group in −N(R)−H has been strategically modified from a strong electron-withdrawing group (e.g., Ts) to a weak electron-withdrawing Ac group and then to the alkyl electron-donating group. This, together with rationally tuning the electron-withdrawing/donating strength of the substituent on the benzene moiety of aniline (see Scheme 1), generates a family of N−H-type intramolecular H-bond compounds that cover a broad range of H-bond strength.

Compared with the ultrafast rate of O−H-type ESIPT, the relatively slow amino N−H ESIPT and the versatility of chemical derivation for the first time offer the advantage of probing correlation among N(R)−H bond distances and proton acidity, ESIPT dynamics, and even thermodynamics. Consequently, it has become feasible to harness ESIPT and hence ratiometric emission for normal versus proton-transfer tautomer fluorescence. Elaborated in the following are details of the synthetic strategy and methodology, substituent effects on the steady-state to femtosecond spectroscopy/dynamics of the ESIPT reaction, and the associated ESIPT−structure relationship.

Synthesis and Characterizations. The parent compound 2-(2′-aminophenyl)benzothiazole (**PBT-NH$_2$**) and its derivatives, 2-(2′-tosylaminophenyl)benzothiazole (**PBT-NHTs**), 2-(2′-acetylaminophenyl)benzothiazole (**PBT-NHAc**), 2-(2′-methylaminophenyl)benzothiazole (**PBT-NHMe**), 2-(5′-cyano-2′-aminophenyl)benzothiazole (**CN-PBT-NH$_2$**), 2-(5′-cyano-2′-tosylaminophenyl)benzothiazole (**CN-PBT-NHTs**), 2-(5′-cyano-2′-methylaminophenyl)benzothiazole (**CN-PBT-NHMe**), and 2-(5′-amino-2′-tosylaminophenyl)benzothiazole (**NH$_2$-PBT-NHTs**), were synthesized. The synthetic routes for these compounds are depicted in Scheme 1. Detailed synthesis and characterizations are provided in the Supporting Information (SI). The N−H deuterated **CN-PBT-NHMe**, **CN-PBT-NH$_2$**, and **PBT-NHAc**, namely, **CN-PBT-NDMe**, **CN-PBT-ND$_2$**, and **PBT-NDAc**, were prepared by dissolving the N−H samples in methanol-*d* (CH_3OD), followed by solvent evaporation. This procedure was repeated more than three times until the deuterated content was >95% monitored by ^{1}H NMR.

Spectroscopic Measurements. Steady-state absorption spectra were recorded using a Hitachi U-3310 spectrophotometer, and emission spectra were obtained using an Edinburgh FS920 fluorometer. Detailed time-resolved spectroscopic measurements have been reported previously.[26] In brief, nanosecond time-resolved experiments were performed by using an Edinburgh FLS920 time-correlated single photon-counting (TCSPC) system with a pulsed hydrogen-filled lamp as the excitation source. Data were fitted with the sum of exponential functions using a nonlinear least-squares procedure in combination with a convolution method.

Subnanosecond to nanosecond time-resolved studies were performed using another TCSPC system (OB-900 L lifetime spectrometer, Edinburgh) with an excitation light source from the second-harmonic generation (SHG, 360 nm) of pulse-selected femtosecond laser pulses at 720 nm (Tsunami, Spectra-Physics). The fluorescence was collected at a right angle with respect to the pump beam path and passed through a polarizer, which was located in front of the detector. The polarization was set at a magic angle (54.7°) with respect to the pump polarization direction to eliminate anisotropy. Similar data analysis and fitting procedures were applied. The temporal resolution, after partial removal of the instrumental time broadening, was ∼50 ps.

Ultrafast spectroscopic study of the titled compounds was performed by a femtosecond photoluminescence up-conversion (uPL) system pumped at 400 nm (for **PBT-NH$_2$**, **PBT-NHMe**, **CN-PBT-NH$_2$**, and **CN-PBT-NHMe**) and at 360 nm (for **PBT-NHTs**, **CN-PBT-NHTs**, **NH$_2$-PBT-NHTs**, and **PBT-NHAc**). The femtosecond oscillator (Tsunami, Spectra-Physics) mentioned in the previous paragraph was used with the central output wavelength at 800 or 720 nm. In this

DOI: 10.1021/acs.jpclett.5b00423
J. Phys. Chem. Lett. 2015, 6, 1477−1486

measurement, fluorescence from a rotating sample cell was focused in a BBO crystal, and its frequency was summed along with an interrogation gate pulse at a designated delay time with respect to the pump pulse. A half-wave plate was used to set the pump polarization at a magic angle (54.7°) with respect to the gate pulse to prevent the fluorescence anisotropy contributed by solute reorientation. Fluorescence up-conversion data were fitted to the sum of exponential functions convoluted with the instrument response function (IRF). The IRF was determined from the Raman scattering signal, and its profile was fitted to a Gaussian function with a full width at half-maximum of ~150 fs.

Computational Methodology. The geometries of the singlet ground states were optimized by the density functional theory (DFT) method, and the excited-state structures and related optical properties of all molecules were calculated with time-dependent density functional theory (TDDFT) methodology with a B3LYP hybrid function in combination with a polarizable continuum model (PCM) in CH_2Cl_2. The 6-311+G(d,p) basis set was employed for all atoms.

The lowest singlet (S_1) excited-state geometries were also optimized by configuration-interaction singles (CIS) theory. Single-point excited-state energies were also calculated using the TD-CAM-B3LYP theory with a 6-311+G(d,p) basis set under the structures optimized at the CIS/6-311+G(d,p) level. All calculations were carried out using the Gaussian 09 program.[27]

Synthesis. Although **PBT-NH$_2$** can be prepared from anthranilic acid according to reported procedures,[28] it is more straightforward and hence efficient to use isatoic anhydride and 2-aminothiophenol under $ZnCl_2$ catalysis (see Scheme 1 and the SI). To tune the proton acidity on the amino group, electron-withdrawing or -donating groups (Ts, Ac, or Me) are introduced onto the amino nitrogen. The prototype **PBT-NH$_2$** is transformed into the sulfonamide compound **PBT-NHTs** by reacting with tosyl chloride (TsCl) in pyridine. Ts is a strong electron-withdrawing group that further lowers the electron density on the N atom, as evidenced by the chemical shift of the sulfonamide proton in **PBT-NHTs**, which is shifted greatly downfield to 12.20 ppm, as compared to 6.38 ppm for the amino proton in **PBT-NH$_2$**. Synthesis of the methylated compound **PBT-NHMe** could be achieved through two pathways. The first option is to allow **PBT-NH$_2$** to react directly with methyl iodide. However, instead of **PBT-NHMe**, we found the major product to be an *N*,*N*′-dimethylated compound. To solve this problem, we then used an alternative route starting from isatoic anhydride. The first step was *N*-methylation, giving *N*-methylisatoic anhydride with a high yield of 91%. The intermediate was then allowed to react with 2-aminothiophenol under a $ZnCl_2$-catalyzed condensation condition to give **PBT-NHMe** with a reasonable yield (54%). The third variation on the amino group is the introduction of an Ac group, which is expected to be a weaker electron-withdrawing group as compared to Ts. As a result, **PBT-NHAc** was obtained in a high yield (96%) through acetylation of **PBT-NH$_2$**.

In addition to the modifications on the amino group, we also functionalized the benzene moiety of aniline to further tune the proton-donating ability. Accordingly, an electron-withdrawing cyano group was introduced via an aromatic *para*-bromination of **PBT-NH$_2$**, followed by copper-assisted cyanation in *N*,*N*-dimethylacetamide (DMAc). The desired product **CN-PBT-NH$_2$** could be obtained, but the yield was not satisfactory. Alternatively, the yield of cyanation can be improved by starting with an iodo- intermediate instead of the bromo- intermediate. The iodo- intermediate I-PBT-NH$_2$ was prepared from **PBT-NH$_2$** by using a mixture of KI and $NaIO_4$ to provide the reactive iodonium cation for iodination. Similar iodination and cyanation procedures led to the successful synthesis of **CN-PBT-NHMe** from **PBT-NHMe**. Sulfonamide **CN-PBT-NHTs** could be obtained by allowing **CN-PBT-NH$_2$** to react with TsCl following the same method described above for **PBT-NHTs**. Finally, the *para*-amino compound **NH$_2$-PBT-NHTs** was prepared from **PBT-NHTs** via nitration, followed by reduction.

Steady-State Spectroscopy. The electronic absorption spectra and steady-state emission spectra for the titled compounds in dichloromethane at room temperature are shown in Figure 1,

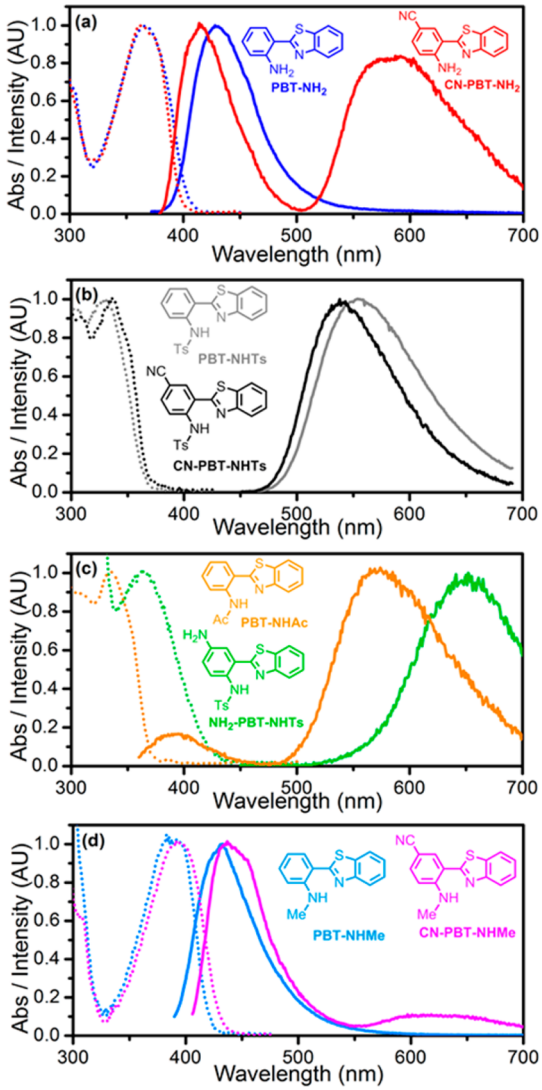

Figure 1. Normalized steady-state absorption spectra (dotted lines) and emission spectra (solid lines) for the titled compounds in CH_2Cl_2 at room temperature.

and pertinent data are presented in Table 1. Similar results were observed in cyclohexane and *n*-hexane. However, the sparse solubility of these compounds in nonpolar solvents makes further femtosecond fluorescence up-conversion measurements infeasible. Therefore, dichloromethane was used as the solvent throughout the spectroscopic studies unless otherwise specified.

DOI: 10.1021/acs.jpclett.5b00423
J. Phys. Chem. Lett. 2015, 6, 1477−1486

Table 1. Observed Steady-State Absorption/Emission Peak Wavelengths (λ_{em}) and Molar Absorptivities (ε) Recorded in CH_2Cl_2 at Room Temperature, Computed Absorption/Emission Wavelengths and Oscillator Strengths (f) of the First Singlet Excitation/Relaxation in Their Normal or Tautomer Forms, and Observed/Computed Corresponding Energy Differences ($\Delta E^* = E^*_{tautomer} - E^*_{normal}$) between the Normal Form and Tautomer Form Species in the Lowest Excited State (S_1) for the Titled Compounds

compound	observed λ_{abs}/nm (ε/M^{-1} cm^{-1})	computed λ_{abs}/nm (f)	observed λ_{em}/nm (Φ_{em})	computed λ_{em}/nm (f)	observed ΔE^*/kcal·mol^{-1}	computed ΔE^*/kcal·mol^{-1}
PBT-NHMe	392 (16600)	391 (0.3955)	458 (3.50%)	431 (0.3706)		7.28
PBT-NH_2	366 (14400)	369 (0.4094)	431 (1.60%)	409 (0.4087)		5.66
CN-PBT-NHMe	393 (15700)	381 (0.3965)	436 (0.69%)	421 (0.4073)	0.14	4.09
			623 (0.15%)	563 (0.2801)		
CN-PBT-NH_2	363 (13900)	364 (0.4302)	419 (0.50%)	402 (0.4844)	−1.07	2.60
			588 (0.50%)	529 (0.3074)		
PBT-NHAc	335 (17900)	347 (0.4906)	395 (0.03%)	393 (0.5463)	−1.53	1.23
			565 (0.16%)	618 (0.0013)		
NH_2-PBT-NHTs	362 (9400)	391 (0.1586)	649 (0.42%)	645 (0.2338)		−1.22
PBT-NHTs	330 (14700)	339 (0.4312)	555 (0.86%)	524 (0.2748)		−6.16
CN-PBT-NHTs	336 (14500)	343 (0.4325)	540 (7.70%)	519 (0.2695)		−7.27

All compounds have similar electronic absorption features, consisting of an intense band peaked in the UV (from 330 to 393 nm) with a molar absorptivity (ε) ranging from 9400 to 17900 M^{-1} cm^{-1}, which is ascribed to the typical $\pi-\pi^*$ transitions. The emission spectrum of **PBT-NH_2** (Figure 1a) shows a band centered at 431 nm with an emission quantum yield (Φ_{em}) of 1.60%. The emission spectrum is a mirror image of the absorption spectrum with a small Stokes shift, defined as the difference between the lowest-lying absorption peak and the emission peak in terms of wavenumber, of <4000 cm^{-1}. Both spectral features suggest that the emission is quite normal, that is, an emission from the relaxed Franck−Condon excited state with no ESIPT taking place. To facilitate proton ESIPT, we then prepared **PBT-NHTs** by adding a Ts group to replace one of the amino protons, forming **PBT-NHTs**. The blue-shifted absorption of **PBT-NHTs** (λ_{abs} = 330 nm, Figure 1b) from **PBT-NH_2** can be attributed to the electron-withdrawing Ts group, which further lowers the HOMO energy (vide infra). As shown in Figure 1b, the emission spectrum of **PBT-NHTs** maximized at 555 nm features an anomalously large Stokes shift of ∼12000 cm^{-1}. This, together with a large separation of spectral onset between absorption and emission unambiguously indicates the occurrence of ESIPT, resulting in a proton-transfer tautomer emission at 555 nm.

When Ts in **PBT-NHTs** was replaced with a weaker electron-withdrawing Ac group, forming **PBT-NHAc**, ESIPT seemed to be retarded, as evidenced by the observation of both normal and tautomer emissions, maximized at 395 and 565 nm, respectively (Figure 1c). We then further introduced an electron-donating methyl group to the amino nitrogen, forming **PBT-NHMe**. The spectrum of **PBT-NHMe** showed a red shift in the absorption peak wavelength (λ_{abs} = 392 nm, Figure 1d) with respect to the parent compound **PBT-NH_2** (Figure 1a). Supported by the later computational approach, this can be rationalized by lifting of the HOMO energy via increasing the electron density from the methyl group. As expected, only one band was present for **PBT-NHMe** (λ_{em} = 458 nm) with a normal Stokes shift of <3500 cm^{-1}, indicating the prohibition of ESIPT. The results on **PBT-NH_2**, **PBT-NHAc**, and **PBT-NHTs** thus drew our attention because the amino proton-donating strength seemed to be altered by the electronic nature of the substituents on the amino group, which consequently affected the driving force of ESIPT.

We then exploited the same tactics and further expanded the scope of the investigation to different substituent domains of the molecules in influencing the corresponding ESIPT properties. Accordingly, instead of modifying the amino nitrogen, we added an electron-withdrawing cyano group on the benzene ring at the para position with respect to the amino group, yielding **CN-PBT-NH_2** (see Scheme 1 and Figure 1a). The introduction of the cyano group did not have a noticeable effect on the absorption as compared to **PBT-NH_2** and **CN-PBT-NH_2** (Figure 1a). However, in stark contrast to the single normal emission band (431 nm) in **PBT-NH_2**, the emission spectrum of **CN-PBT-NH_2** consists of two distinctly separated emission bands with peaks at 419 and 588 nm in CH_2Cl_2, which are ascribed to normal and proton-transfer tautomer emission, respectively. Such a tuning from non-ESIPT (**PBT-NH_2**) to ESIPT (**CN-PBT-NH_2**) grants us new control over the ESIPT reaction.

Subsequently, upon modifying both the para position on the benzene ring and the amino nitrogen by adding −CN and −Ts, respectively, to form **CN-PBT-NHTs**, we would expect a full proton transfer because both electron-withdrawing −CN and −Ts groups show positive effects on ESIPT. As a result, the emission spectrum of **CN-PBT-NHTs** (Figure 1b) agreed well with the prediction, showing solely the proton-transfer tautomer emission with a peak wavelength at 540 nm. In light of this trend, it is interesting to examine the ESIPT property upon the addition of the *para*-cyano group to the non-ESIPT molecule **PBT-NHMe**, which possesses the weakest amino proton-donating strength. The resulting **CN-PBT-NHMe** exhibits a distinct tautomer emission at 623 nm in addition to the 436 nm normal emission (Figure 1d), proving that the electron-withdrawing group again helps to facilitate ESIPT for **CN-PBT-NHTs**, as opposed to the strictly non-proton-transfer molecule **PBT-NHMe**.

Finally, compound **NH_2-PBT-NHTs** was also synthesized. In this compound, an electron-donating amino group was added at the para position with respect to the −NHTs site of **PBT-NHTs**, with the aim of examining whether proton transfer could be slowed from the otherwise full ESIPT in **PBT-NHTs**.

DOI: 10.1021/acs.jpclett.5b00423
J. Phys. Chem. Lett. 2015, 6, 1477−1486

Unfortunately, similar to that of **PBT-NHTs**, **NH_2-PBT-NHTs** shows solely the tautomer emission (Figure 1c). From the viewpoint of chemistry, qualitatively, the result implies that the electron-donating strength of the *para*-amino group is not strong enough to compete with the electron-withdrawing power of the Ts group. Further firm support of the above steady-state spectroscopy, that is, the intensity ratio for the normal versus tautomer emission, is provided in the time-resolved emission kinetics elaborated below.

Time-Resolved Emission Kinetics. Fluorescence up-conversion and TCSPC techniques (see the experimental details) were then used in probing the excited-state dynamics of the titled compounds. On the one hand, for **PBT-NHTs**, **CN-PBT-NHTs**, and **NH_2-PBT-NHTs** showing exclusively proton-transfer tautomer emission, the fluorescence lifetimes were obtained and are listed in Table 2. The population decay kinetics recorded using TCSPC and the early emission kinetics acquired by the uPL technique are revealed in Figure 2a for the representative compound **PBT-NHTs**. Apparently, the rise time of the proton-transfer tautomer emission was irresolvable (Figure 2a inset), indicating that the ESIPT rate was ultrafast and beyond our IRF (~150 fs). Similar system-response-limited ESIPT kinetics were observed for **CN-PBT-NHTs** and **NH_2-PBT-NHTs**. On the other hand, for the presence of dual emissions in **CN-PBT-NHMe**, **CN-PBT-NH_2**, and **PBT-NHAc**, detailed analyses revealed the coexistence of normal and tautomer forms in their excited state and under equilibrium. Representative emission kinetic traces for **CN-PBT-NHMe** in CH_2Cl_2 are presented in Figure 2b. For **PBT-NH_2** and **PBT-NHMe** that do not show proton transfer, both their normal form emissions decay biexponentially. This is likely due to the coexistence of the species with and without the intramolecular H-bond.

For **CN-PBT-NHMe** in CH_2Cl_2, the normal form emission monitored at 460 nm decays biexponentially with lifetimes of 2.31 and 43.0 ps, while the tautomer emission at 620 nm consists of a 2.10 ps rise time component and a decay time of 43.8 ps (Figure 2b and Table 2). Within experimental error, the shorter decay component (2.31 ps) of the normal emission and the rise (2.10 ps) of the tautomer emission are well-matched with the opposite sign for the pre-exponential factor. The result clearly concludes a precursor (normal)−successor (tautomer) type of ESIPT in the early stage. Another remarkable observation was the identical population decay times of both normal and tautomer emissions, ~43 ps. The combination of these observations leads us to conclude the occurrence of ESIPT, followed by a fast pre-equilibrium between normal and tautomer in the excited state prior to the occurrence of each individual emission decay.

The corresponding reaction kinetics can be described by a coupling reaction model depicted in Scheme 2, with a kinetic expression for the concentrations of both the excited-state normal form ([N*]) and tautomer form ([T*]) shown in eqs 1 and 2.

$$\frac{d[N^*]}{dt} = -(k_{N^*} + k_{pt})\cdot[N^*] + k_{-pt}\cdot[T^*] \quad (1)$$

$$\frac{d[T^*]}{dt} = -(k_{T^*} + k_{-pt})\cdot[T^*] + k_{pt}\cdot[N^*] \quad (2)$$

Table 2. Observed Emission Lifetimes (τ_{obs}) for the Proton-Transfer Compounds in CH_2Cl_2 at Room Temperature

compound	$\lambda_{monitor}$/nm	τ_{obs} by uPL (pre-exp. factor)
PBT-NHTs	580	712 ps[a]
CN-PBT-NHTs	580	4.17 ns[b]
NH_2-PBT-NHTs	600	53.9 ps
CN-PBT-NHMe	460	2.31 ps (0.44)
		43.0 ps (0.56)
	620	2.10 ps (−0.39)[c]
		43.8 ps (0.61)
CN-PBT-NH_2	460	5.25 ps (0.86)
		68.0 ps (0.14)
	620	5.20 ps (−0.46)[c]
		64.0 ps (0.54)
PBT-NHAc	430	0.39 ps (0.93)
		33.7 ps (0.07)
	600	0.41 ps (−0.44)[c]
		35.3 ps (0.56)
PBT-NH_2	460	12.6 ps (0.26)
		52.8 ps (0.74)
PBT-NHMe	480	22.0 ps (0.32)
		288 ps (0.68)

[a]The lifetime was measured using a TCSPC system with femtosecond excitation pulses. [b]Lifetime measured using a TCSPC system with a pulsed hydrogen-filled lamp as the excitation source. [c]Rise kinetics.

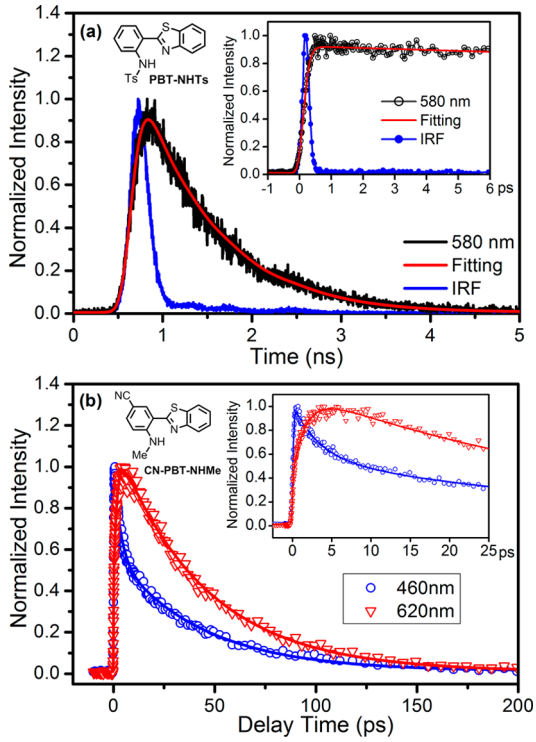

Figure 2. (a) Population decay kinetic trace (black) at 580 nm acquired by TCSPC for **PBT-NHTs** in CH_2Cl_2 at room temperature. The sample was excited at 360 nm. (Inset) uPL kinetic traces (λ_{ex} = 360, λ_{em} = 580 nm). The IRF (blue) and fitting curves (red) are also included for both plots. (b) uPL kinetic traces for **CN-PBT-NHMe** in CH_2Cl_2. The sample was excited at 400 nm, and emission kinetic data were collected at 460 and 620 nm for the normal and tautomer emissions, respectively. Solid lines depict the best fits using eq 3. The fitting data are summarized in Table 2. (Inset) The enlargement of kinetic traces from 0 to 25 ps.

DOI: 10.1021/acs.jpclett.5b00423
J. Phys. Chem. Lett. 2015, 6, 1477−1486

Scheme 2. Pre-equilibrium Model for the Amino-Type ESIPT[a]

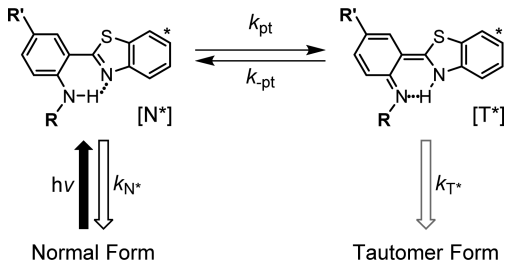

[a]Here, [N*] and [T*] are the concentrations of the excited-state normal and tautomer form species; k_{N^*} and k_{T^*} are the decay rate constants for N* and T*; k_{pt} and k_{-pt} are the forward and backward proton-transfer rates, respectively.

The two differential equations eqs 1 and 2 can be solved,[29] giving a fitting equation for the fluorescence kinetics, expressed as eq 3.

$$I(t) = A_1 \cdot e^{-t/\tau_1} + A_2 \cdot e^{-t/\tau_2} \quad (3)$$

Here, $I(t)$ is the fluorescence intensity as a function of time, which is also proportional to [N*](t) and [T*](t). τ_1 and τ_2 are the observed relaxation times. A_1 and A_2 are the pre-exponential factors, which under the pre-equilibrium of ESIPT then correlate to eq 3 to give the relations in eqs 4 and eq 5 for the normal emission.

$$A_1 \approx \frac{k_{-pt}}{k_{pt} + k_{-pt}} \quad (4)$$

$$A_2 \approx \frac{k_{pt}}{k_{pt} + k_{-pt}} \quad (5)$$

As a result, the equilibrium constant K_{eq} ($= k_{pt}/k_{-pt} = A_2/A_1$) is then deduced to be 0.79, which corresponds to an endergonic ESIPT reaction ΔG = 0.14 kcal/mol for **CN-PBT-NHMe**. Because $K_{eq} = k_{pt}/k_{-pt}$ and $k_{pt} + k_{-pt} = 1/\tau_1$,[29] the forward and backward proton-transfer rate constants can be derived to be $k_{pt} = 1.3 \times 10^{11}$ s^{-1} and $k_{-pt} = 1.7 \times 10^{11}$ s^{-1}.

Similar behavior of excited-state equilibrium was observed for **CN-PBT-NH$_2$** in CH_2Cl_2. As listed in Table 2, the 5.25 ps fast decay for the normal form emission monitored at 460 nm is virtually the same as the 5.20 ps rise of the tautomer emission monitored at 620 nm, and the population decay of normal (68.0 ps) and tautomer (64.0 ps) emission, within experimental error, is considered to be identical. Using these experimental data, $k_{pt} = 1.6 \times 10^{11}$ s^{-1}, $k_{-pt} = 2.7 \times 10^{10}$ s^{-1}, $K_{eq} = 6.1$, and $\Delta G = -1.07$ kcal/mol can thus be deduced. As for **PBT-NHAc**, the normal emission decays biexponentially with lifetimes of 0.39 and 33.7 ps, which correlate well with the tautomer emission kinetics of a 0.41 ps rise and a 35.3 ps decay. K_{eq} is thus calculated to be 13 ($k_{pt} = 2.4 \times 10^{12}$ s^{-1} and $k_{-pt} = 1.8 \times 10^{11}$ s^{-1}), corresponding to a ΔG of −1.53 kcal/mol. In sum, the ESIPT process is slightly endergonic for **CN-PBT-NHMe** and exergonic for **CN-PBT-NH$_2$** and **PBT-NHAc** in CH_2Cl_2.

We also performed the uPL experiments for the N−H deuterated compounds, namely, **CN-PBT-NDMe**, **CN-PBT-ND$_2$**, and **PBT-NDAc**, in dry dichloromethane. The representative kinetic traces of **CN-PBT-NDMe**, together with that of the nondeuterated **CN-PBT-NHMe**, are shown in Figure S1 (SI). All pertinent kinetic data are listed in Table S4 (SI). Careful analyses indicate that, within experimental error, the resolved kinetic traces between deuterated and nondeuterated compounds are identical. The lack of kinetic isotope effect implies that the ESIPT process of the titled compounds is not likely to be the direct migration of the proton (tunnelling) but instead is more plausibly induced by the change of the molecular skeleton associated with the H-bond (distance and/or angle), so that the proton donor and acceptor can approach each other prior to proton transfer.[3]

Thermodynamics versus Kinetics of the Amino ESIPT Reactions. The kinetic data deduced above are consistent with normal versus proton-transfer tautomer emission observed in the steady-state measurement for the titled compounds. More importantly, together with other physical parameters elaborated below, there exists an empirical correlation among proton-donating strength, reaction kinetics, and thermodynamics for this series of amino-type ESIPT molecules.

Prior to discussion, we carried out a computational approach (see the experimental details for details) to shed light on the ESIPT energetics in this series of amino-type systems. For all titled compounds, the computed lowest-lying electronic transition ($S_0 \rightarrow S_1$) in terms of wavelength agrees well with the experimental results (see Table 1), supporting the validity of the current computational approach. Also, using representative compounds **PBT-NHTs** and **CN-PBT-NHMe** as examples (frontier orbitals shown in Table 3), by and large, the HOMO commonly possesses a higher electron density on the amino group than the LUMO, whereas an increase in the electron density on the N atom of the benzothiazole domain is generally observed from HOMO to LUMO. Accordingly, the charge-transfer character upon HOMO−LUMO transitions, especially the shift of electron density from the amino N atoms to the benzothiazole N atoms, serves as a driving force for ESIPT. The overall charge-transfer character in the transition is not significant, which can be supported by the following facts: (1) The electron density in both HOMO and LUMO is spread across the entire molecular skeleton (Tables 3 and S1 (SI)), and (2) the normal emission shows very minor solvatochromism (see Figure S2, SI, using **CN-PBT-NHMe** as an example).

Table 3. Computed Frontier Orbitals for PBT-NHTs and CN-PBT-NHMe in Their Normal Form Involved in the First Singlet Excitation[a]

Compound	Structure	HOMO	LUMO
PBT-NHTs	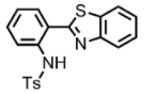	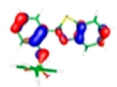	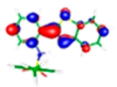
CN-PBT-NHMe	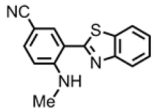	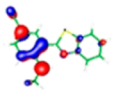	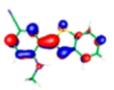

[a]See Table S1 (SI) for a full list of the frontier orbitals for the titled compounds.

For all the titled compounds, we then calculated the ground-state (S_0) energies and the first excited-state (S_1) energies for both the normal and proton-transfer tautomer under the corresponding optimized geometry. Accordingly, the energy difference between the excited-state normal and tautomer forms, $\Delta E^* = E^*_{tautomer} - E^*_{normal}$, for the ESIPT process are shown in Table 1 (the asterisk denotes the excited state). For

DOI: 10.1021/acs.jpclett.5b00423
J. Phys. Chem. Lett. 2015, 6, 1477−1486

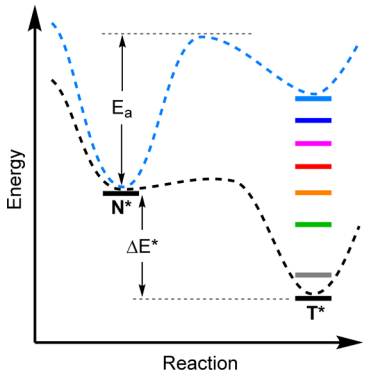

	ΔE* (kcal/mol)		k_{pt}
	Computed	Observed	
PBT-NHMe	7.28		No PT
PBT-NH_2	5.66		No PT
CN-PBT-NHMe	4.09	0.14	1.3 x 10^{11} s^{-1}
CN-PBT-NH_2	2.60	-1.07	1.6 x 10^{11} s^{-1}
PBT-NHAc	1.23	-1.53	2.4 x 10^{12} s^{-1}
NH_2-PBT-NHTs	-1.22		Ultrafast
PBT-NHTs	-6.16		Ultrafast
CN-PBT-NHTs	-7.27		Ultrafast

Figure 3. Thermodynamics and kinetics correlations for the N−H-type ESIPT reactions in the titled compounds. Here, ΔE^* is the energy difference between the N* and T* states, E_a is the activation energy, and k_{pt} is the proton-transfer rate constant. Note that the potential energy curves (dashed lines) drawn for the ESIPT reactions are only qualitative.

more detailed computational results on the energy differences, please see Table S2 (SI).

Computation and spectroscopy results were combined to establish the thermodynamic trends of the titled compounds, classified into three categories: (1) The calculated highly endothermic reactions ($\Delta E^* > 5$ kcal/mol) for **PBT-NHMe** and **PBT-NH_2** are consistent with the prohibition of ESIPT; hence, only normal emission can be observed experimentally. (2) The calculated ΔE^* of around 1.23−4.09 kcal/mol for **CN-PBT-NMe**, **CN-PBT-NH_2**, and **PBT-NHAc**, within uncertainty, may correlate with their equilibrium type of ESIPT and hence dual emission. (3) The calculated exothermic ESIPT reactions ($\Delta E^* < 0$) for **NH_2-PBT-NHTs**, **PBT-NHTs**, and **CN-PBT-NHTs** seem to match well with their ultrafast ESIPT, resulting solely in tautomer emission. Thus, the correlation between this thermodynamic trend and other crucial parameters for ESIPT is feasible.

Chemically, the occurrence of ESIPT requires that the intramolecular H-bond consists of a proton-donating site and a proton-accepting site. For long, this prerequisite has been one of the core fundamental issues regarding the trend of ESIPT and its correlation with the strength of proton-donor/acceptor capabilities and hence the associated H-bond properties. Experimentally, this is still a formidable task, mainly due to the lack of suitable ESIPT systems, for which the corresponding ESIPT dynamics could be carried out in a systematic and comprehensive manner. Most ESIPT systems involve a hydroxyl proton, which under the perturbation free condition (vide infra) undergoes either barrierless, that is, an adiabatic, coherent type of ESIPT or ESIPT with a rather small barrier, such that any vibration associated with the changes of the H-bond distance/orientation may lower or modulate the barrier, inducing the reaction. For the former, oscillation of the tautomer emission, that is, a quantum beat pattern, associated with the coherent motion, has been occasionally observed.[30] These systems all involve strong intramolecular H-bonding; therefore, ESIPT may be described virtually as a wave function redistribution rather than nuclear motion, that is, proton or hydrogen atom motion. As a result, the rate of ESIPT in most cases is within or beyond the system detection response limit (e.g., ≪1 ps). Such an ultrafast, irresolvable time scale made the study of the ESIPT versus structure relationship unattainable.

On the other hand, under external perturbations, the rate of ESIPT could be greatly slowed. For example, in protic solvents, the external H-bond from solvent molecules may drastically alter/reduce the rate of ESIPT. Also, proton transfer may couple with substantial electron-transfer character, such that there is a substantial change of dipole moment from the reactant (the excited-state normal form species) to the product (the excited-state tautomer species), in essence being quite different in their equilibrium polarization. In this case, amid ESIPT, the solvent has to be reorganized, bringing both the reactant and the product to a resonance prior to proton transfer. Therefore, there exists a solvent-polarity-induced barrier that will channel into the ESIPT reaction, giving a finite reaction rate. These two factors unfortunately provide an irrelevant relationship with respect to the proton-donor/acceptor properties. In our view, unavoidably, the correlation should be established under the intrinsically slow, resolvable ESIPT. From a chemical point of view, in other words, we might be able to look for a weak proton donor or acceptor to reduce the driving force of ESIPT. Moreover, and more difficult, the strength of the proton donor (i.e., acidity) or the proton acceptor (i.e., basicity) has to be systematically fine-tuned to probe the ESIPT−H-bond strength relationship.

Apparently, ESIPT systems that can fulfill these two criteria are so rare that relevant studies are still lacking at this stage. In this regard, the new series of amino-type proton donors presented here shine a light on manipulating ESIPT reactions by tuning the intrinsic properties of the molecules. One of the most important observations in this study is the trend of the ESIPT rates and the energy differences (ΔE^*) between the excited-state normal (N*) and tautomer (T*) forms. Conventionally, ΔE^* between the product (T* in this case) and the reactant (N* in this case) determines whether T* could be produced thermodynamically, whereas the rate of ESIPT is generally irrelevant to ΔE^* and is manipulated by the way of forming an activated complex, that is, a transition state. Because all of the titled amino-type compounds have highly similar molecular structures and therefore are expected to undergo similar ESIPT reaction pathways, we then attempted to find a correlation between thermodynamics (ΔE^*) and the forward reaction rate of ESIPT listed in Figure 3. For the convenience of the reader, Figure 3 also draws tentative potential energy curves of the ESIPT reaction for the titled compounds in a very qualitative manner. In Figure 3, for those ESIPT systems under excited-state equilibrium, the experimentally observed thermodynamics data are also included. The combination of experimental and computational data indicates that when ΔE^* becomes more negative, the ESIPT rate increases accordingly.

DOI: 10.1021/acs.jpclett.5b00423
J. Phys. Chem. Lett. 2015, 6, 1477−1486

We then looked into the correlation between ΔE^* and other factors, such as proton acidity. Experimentally, we were unable to measure the acidity of the N−H protons in the titled compounds due to the sparse solubility of the samples in water. However, we were able to obtain the ^{1}H NMR chemical shifts of the N−H protons in $CDCl_3$ (Table S3, SI). The more deshielded protons are usually downfield with more positive chemical shifts and are conventionally considered to be more acidic. We also plotted the chemical shifts as a function of ΔE^* of ESIPT; the result shown in Figure 4a reveals a trend that more acidic protons (with more positive chemical shifts) lead to more thermodynamically favored ESIPT reactions (i.e., with a more negative ΔE^*).

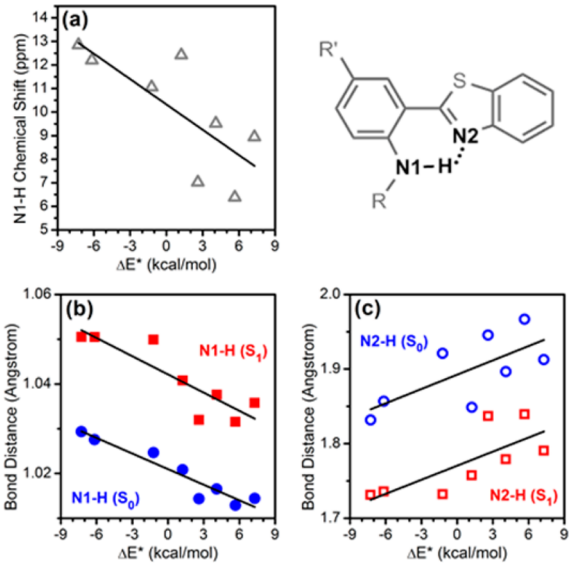

Figure 4. Correlation plots between the computed energy difference ΔE^* and (a) the ^{1}H NMR chemical shift for N1−H in $CDCl_3$, (b) the computed N1−H bond distances in the S_0 or S_1 states, and (c) the computed N2−H bond distances in the S_0 or S_1 states. Here, N1 is the amino N atom, and N2 is the benzothiazole N atom, as shown in the structure to the upper right.

Viewing this phenomenon from another angle, we then computed the N1−H and N2−H bond distances for the title compounds in both the ground (S_0) and the first excited (S_1) states (Table S3, SI), in which N1 and N2 denote the amino nitrogen atom and the benzothiazole nitrogen atom, respectively (see Figure 4, upper right for the notation). Upon plotting the bond distances versus ΔE^*, we perceived a trend that the longer N1−H bond distances in the ground state lead to a more negative ΔE^* (Figure 4b, N1−H (S_0), blue dots), and coherently, N2−H (S_0) decreases when ΔE^* becomes more negative (Figure 4c, blue circles). In the S_1 state, although the N1−H bond distances increase (Figure 4b, N1−H (S_1), red squares) and the N2−H bond distances decrease (Figure 4c, N2−H (S_1), red open squares), both still show a trend (i.e., the correlation of bond distance versus ΔE^*) similar to that of the ground state. In brief, the N1−H (S_0) bond distances and the proton acidity/chemical shifts (Figure 4a) reveal the same trend. All of these results suggest that by rationally modifying the molecules with either electron-withdrawing or -donating groups, one can harness the proton-transfer reaction, or the rate and ΔE^* of ESIPT, by manipulating the related physical parameters, including proton acidity, H-bond distances, and proton-transfer rates, all of which seem to be well-correlated with each other.

The above multiple correlations, on the one hand, may be rationalized by considering proton transfer as an acid−base type of thermodynamic property, in which the stronger N−H proton-donating strength leads to higher acidity and thus greater exergonic ESIPT reaction. On the other hand, among the titled compounds, those possessing relatively weak amino-type H-bonding (cf. the −OH-type H-bond system) require adjustment of the geometry associated with the H-bond to trigger ESIPT. Accordingly, a non-negligible barrier is thus induced amid the H-bond optimization. A stronger H-bond endowed with a shorter bond distance results in a smaller geometry adjustment and hence a smaller ESIPT barrier. For the titled amino-type compounds, such a relationship fortunately can be resolved with both spectroscopy and dynamics approaches due to the relatively weak amino-type H-bond and the full capability of chemical modification on the amino proton, which is otherwise impossible in the traditional −OH type of ESIPT systems.

In summary, a comprehensive photophysical study has been carried out on a new class of amino-type H-bonding compounds with the aim of shedding light on the relationships among ESIPT kinetics, thermodynamics, and the associated H-bond properties. ESIPT in the parent molecules **PBT-NH$_2$** and **PBT-NHMe** is highly endergonic and thus prohibited. In the presence of strong electron-withdrawing Ts that directly replaces one of the amino protons, complete and ultrafast (τ_{pt} < 150 fs) ESIPT is thus resolved for **PBT-NHTs**, **CN-PBT-NHTs**, and **NH$_2$-PBT-NHTs**. Upon the substitution of moderate strong proton-donating groups, compounds **CN-PBT-NMe**, **CN-PBT-NH$_2$**, and **PBT-NHAc** exhibit equilibrium-type ESIPT, resulting in a remarkable dual emission.

The most important observation in this work is the thermodynamic−kinetic relationship because both are also further correlated with the proton-donating strength and hence the H-bond strength/distance. On the one hand, such a correlation can be rationalized by treating the proton-transfer reaction as an acid−base type of thermodynamic property, in which the stronger N−H proton-donating strength leads to higher acidity and thus a more exergonic ESIPT reaction. On the other hand, this acid−base property also correlates well with the H-bond distance. For a weak intramolecular H-bond system such as the titled amino-type molecules, the geometry adjustment seems to be a prerequisite for the H-bond to be at a suitable distance to bring resonance, that is, to undergo ESIPT. The stronger H-bond empirically leads to a smaller geometry adjustment and hence a smaller barrier, which correlates with the faster rate of ESIPT.

The proton-transfer reaction can be described by a strong coupling between reactant and product electronic states, which has significant dependence on the distance between the proton donor and acceptor, that is, the H-bonding length. The larger electronic coupling not only reduces the barrier height but also narrows the width. Compared to the nonadiabatic electron transfer, the tunneling probability in nonadiabatic proton transfer should be much more sensitive to interatomic separation simply because the proton is much heavier than the electron, approximately ∼2000 times, which does warrant us to pursue their corresponding fundamental. If so, the empirical rule can be elegantly exemplified by the fundamental N−H proton transfer, which is unprecedented and is otherwise impossible for the typical −OH type of ESPT due to the

DOI: 10.1021/acs.jpclett.5b00423
J. Phys. Chem. Lett. 2015, 6, 1477−1486

ultrafast and hence irresolvable reaction rate as well as the impossibility in fine-tuning the O−H activity by O-substitutions.

Last but not least, in addition to the above fundamental importance, from the aspect of application, we would like to remark that the equilibrium amino-type ESIPT compound, for example, **CN-PBT-NHMe**, results in both normal (420−570 nm) and proton-transfer tautomer (570−725 nm) emission, creating the appearance of white light generation (see Figure S3, SI). The facile tuning of the ESIPT thermodynamics on the amino-type ESIPT systems may thus pave a new avenue for full color tunability in lighting applications.

■ ASSOCIATED CONTENT

Supporting Information

Detailed synthesis and characterizations of compounds, computations, and supplementary photophysics are provided. This material is available free of charge via the Internet at http://pubs.acs.org.

■ AUTHOR INFORMATION

Corresponding Authors

*E-mail: chop@ntu.edu.tw (P.-T.C.).
*E-mail: chimin.chau@gmail.com (C.-M.C.).
*E-mail: lkm@csmu.edu.tw (K.-M.L.).

Notes

The authors declare no competing financial interest.

■ ACKNOWLEDGMENTS

We gratefully acknowledge funding support from the Ministry of Science and Technology, Taiwan. P.-T.C. thanks National Taiwan University, and C.-M.C. and K.-M.L. thank Chung Shan Medical University for financial support.

■ REFERENCES

(1) Chou, P.-T. The Host/Guest Type of Excited-State Proton Transfer; A General Review. *J. Chin. Chem. Soc.* **2001**, *48*, 651−682.
(2) Kwon, J. E.; Park, S. Y. Advanced Organic Optoelectronic Materials: Harnessing Excited-State Intramolecular Proton Transfer (ESIPT) Process. *Adv. Mater.* **2011**, *23*, 3615−3642.
(3) Demchenko, A. P.; Tang, K.-C.; Chou, P.-T. Excited-State Proton Coupled Charge Transfer Modulated by Molecular Structure and Media Polarization. *Chem. Soc. Rev.* **2013**, *42*, 1379−1408.
(4) Carter, T. P.; Van Benthem, M. H.; Gillispie, G. D. Fluorescence and Fluorescence Excitation Spectra of 1-Aminoanthraquinone in an *n*-Heptane Shpol'skii Matrix. *J. Phys. Chem.* **1983**, *87*, 1891−1898.
(5) Allen, N. S.; Harwood, B.; McKellar, J. F. Lightfastness and Spectroscopic Properties of N-Substituted 1-Aminoanthraquinones. *J. Photochem.* **1979**, *10*, 187−192.
(6) Allen, N. S.; Harwood, B.; McKellar, J. F. Lightfastness and Spectroscopic Properties of Aminocarboxyanthraquinones. *J. Photochem.* **1979**, *10*, 193−197.
(7) Smith, T. P.; Zaklika, K. A.; Thakur, K.; Barbara, P. F. Excited-State Intramolecular Proton-Transfer in 1-(Acylamino)-anthraquinones. *J. Am. Chem. Soc.* **1991**, *113*, 4035−4036.
(8) Santra, S.; Krishnamoorthy, G.; Dogra, S. K. Excited State Intramolecular Proton Transfer in 2-(2′-Benzamidophenyl)-benzimidazole: Effect of Solvents. *Chem. Phys. Lett.* **1999**, *311*, 55−61.
(9) Fahrni, C. J.; Henary, M. M.; Van Derveer, D. G. Excited-State Intramolecular Proton Transfer in 2-(2′-Tosylaminophenyl)-benzimidazole. *J. Phys. Chem. A* **2002**, *106*, 7655−7663.
(10) Nayak, M. K. Synthesis, Characterization and Optical Properties of Aryl and Diaryl Substituted Phenanthroimidazoles. *J. Photochem. Photobiol., A* **2012**, *241*, 26−37.
(11) Ciuciu, A. I.; Skonieczny, K.; Koszelewski, D.; Gryko, D. T.; Flamigni, L. Dynamics of Intramolecular Excited State Proton Transfer in Emission Tunable, Highly Luminescent Imidazole Derivatives. *J. Phys. Chem. C* **2013**, *117*, 791−803.
(12) Santra, S.; Krishnamoorthy, G.; Dogra, S. K. Excited-State Intramolecular Proton Transfer in 2-(2′-Acetamidophenyl)-benzimidazole. *J. Phys. Chem. A* **2000**, *104*, 476−482.
(13) Joule, J. A.; Mills, K. *Heterocyclic Chemistry*, 5th ed.; Wiley-Blackwell: West Sussex, U.K., 2010.
(14) Haynes, W. M. *CRC Handbook of Chemistry and Physics*, 95th ed.; CRC Press: Boca Raton, FL, 2014; pp 5−97.
(15) Rodriguez-Prieto, F.; Penedo, J. C.; Mosquera, M. Solvent Control of Molecular Structure and Excited-State Proton-Transfer Processes of 1-Methyl-2-(2′-hydroxyphenyl)benzimidazole. *J. Chem. Soc., Faraday Trans.* **1998**, *94*, 2775−2782.
(16) Vazquez, S. R.; Rodriguez, M. C. R.; Mosquera, M.; Rodriguez-Prieto, F. Excited-State Intramolecular Proton Transfer in 2-(3′-Hydroxy-2′-pyridyl)benzoxazole. Evidence of Coupled Proton and Charge Transfer in the Excited State of Some *o*-Hydroxyarylbenzazoles. *J. Phys. Chem. A* **2007**, *111*, 1814−1826.
(17) Vazquez, S. R.; Rodriguez, M. C. R.; Mosquera, M.; Rodriguez-Prieto, F. Rotamerism, Tautomerism, and Excited-State Intramolecular Proton Transfer in 2-(4′-*N*,*N*-Diethylamino-2′-hydroxyphenyl)-benzimidazoles: Novel Benzimidazoles Undergoing Excited-State Intramolecular Coupled Proton and Charge Transfer. *J. Phys. Chem. A* **2008**, *112*, 376−387.
(18) Tsai, H.-H. G.; Sun, H.-L. S.; Tan, C.-J. TD-DFT Study of the Excited-State Potential Energy Surfaces of 2-(2′-Hydroxyphenyl)-benzimidazole and Its Amino Derivatives. *J. Phys. Chem. A* **2010**, *114*, 4065−4079.
(19) Yang, G.; Dreger, Z. A.; Li, Y.; Drickamer, H. G. Pressure-Induced Isomerization of 2-(2′-Hydroxyphenyl)benzoxazole in Solid Media. *J. Phys. Chem. A* **1997**, *101*, 7948−7952.
(20) Wang, H.; Zhang, H.; Abou-Zied, O. K.; Yu, C.; Romesberg, F. E.; Glasbeek, M. Femtosecond Fluorescence Upconversion Studies of Excited-State Proton-Transfer Dynamics in 2-(2′-Hydroxyphenyl)-benzoxazole (HBO) in Liquid Solution and DNA. *Chem. Phys. Lett.* **2003**, *367*, 599−608.
(21) Chu, Q.; Medvetz, D. A.; Pang, Y. A Polymeric Colorimetric Sensor with Excited-State Intramolecular Proton Transfer for Anionic Species. *Chem. Mater.* **2007**, *19*, 6421−6429.
(22) Kim, C. H.; Park, J.; Seo, J.; Park, S. Y.; Joo, T. Excited State Intramolecular Proton Transfer and Charge Transfer Dynamics of a 2-(2′-Hydroxyphenyl)benzoxazole Derivative in Solution. *J. Phys. Chem. A* **2010**, *114*, 5618−5629.
(23) Rodembusch, F. S.; Campo, L. F.; Stefani, V.; Rigacci, A. The First Silica Aerogels Fluorescent by Excited State Intramolecular Proton Transfer Mechanism (ESIPT). *J. Mater. Chem.* **2005**, *15*, 1537−1541.
(24) Zheng, J. J.; Guo, Y. X.; Li, X. P.; Zhang, G. L.; Chen, W. J. Two-Photon-Induced Excited State Intramolecular Proton Transfer Process and Nonlinear Optical Properties of HBT in Cyclohexane Solution. *J. Opt. A: Pure Appl. Opt.* **2006**, *8*, 835−839.
(25) Wang, R. J.; Liu, D.; Xu, K.; Li, J. Y. Substituent and Solvent Effects on Excited State Intramolecular Proton Transfer in Novel 2-(2′-Hydroxyphenyl)benzothiazole Derivatives. *J. Photochem. Photobiol., A* **2009**, *205*, 61−69.
(26) Chou, P.-T.; Pu, S.-C.; Cheng, Y.-M.; Yu, W.-S.; Yu, Y.-C.; Hung, F.-T.; Hu, W.-P. Femtosecond Dynamics on Excited-State Proton/Charge-Transfer Reaction in 4′-*N*,*N*-Diethylamino-3-hydroxyflavone. The Role of Dipolar Vectors in Constructing a Rational Mechanism. *J. Phys. Chem. A* **2005**, *109*, 3777−3787.
(27) Frisch, M. J.; Trucks, G. W.; Schlegel, H. B.; Scuseria, G. E.; Robb, M. A.; Cheeseman, J. R.; Scalmani, G.; Barone, V.; Mennucci, B.; Petersson, G. A.; et al. *Gaussian 09*, revision A.02; Gaussian, Inc.: Wallingford, CT, 2009.
(28) Meghdadi, S.; Amirnasr, M.; Ford, P. C. A Robust One-Pot Synthesis of Benzothiazoles from Carboxylic Acids Including Examples

DOI: 10.1021/acs.jpclett.5b00423
J. Phys. Chem. Lett. 2015, 6, 1477−1486

with Hydroxyl and Amino Substituents. *Tetrahedron Lett.* **2012**, *53*, 6950−6953.
(29) Tang, K.-C.; Chang, M.-J.; Lin, T.-Y.; Pan, H.-A.; Fang, T.-C.; Chen, K.-Y.; Hung, W.-Y.; Hsu, Y.-H.; Chou, P.-T. Fine Tuning the Energetics of Excited-State Intramolecular Proton Transfer (ESIPT): White Light Generation in A Single ESIPT System. *J. Am. Chem. Soc.* **2011**, *133*, 17738−17745.
(30) Hsieh, C.-C.; Chou, P.-T.; Shih, C.-W.; Chuang, W.-T.; Chung, M.-W.; Lee, J.; Joo, T. Comprehensive Studies on an Overall Proton Transfer Cycle of the *ortho*-Green Fluorescent Protein Chromophore. *J. Am. Chem. Soc.* **2011**, *133*, 2932−2943.

DOI: 10.1021/acs.jpclett.5b00423
J. Phys. Chem. Lett. 2015, 6, 1477−1486